

# Contribution of Hydrogen Molecular Activated Recombination to Plasma Particle Loss in DT-ALPHA

Keigo YOSHIMURA<sup>1)\*</sup>, Hiroyuki TAKAHASHI<sup>1)</sup>, Ryota NISHIMURA<sup>1)</sup>, Tomoya HARA<sup>1)</sup>, Shigetaka KAGAYA<sup>1)</sup>, Tetsutarou OISHI<sup>1)</sup>, Akinobu MATSUYAMA<sup>2)</sup>, Kenji TOBITA<sup>1)</sup>

<sup>1)</sup> Department of Quantum Science and Energy Engineering, Tohoku University, Sendai 980-8579, Japan

<sup>2)</sup> Graduate School of Energy Science, Kyoto University, Uji 611-0011, Japan

(Received 17 July 2024 / Accepted 2 December 2024)

A hydrogen secondary gas feeding experiment was conducted with hydrogen plasma. A rollover of the electron density and a monotonic decrease in the electron temperature were observed as the amount of the secondary gas increased. The vibrational distribution and temperature of ground electronic hydrogen molecules were evaluated based on the Fulcher- $\alpha$  band spectroscopy. To analyze the contribution of molecular activated recombination (MAR) to plasma particle loss, the reaction rates of the dissociative attachment (DA) and ion conversion (IC) of vibrationally excited hydrogen molecules were calculated. The reaction rate of IC was approximately two orders of magnitude greater than that of DA and significantly increased with the onset of the density rollover. The IC reaction rate remained high even as the electron density decreased. This analysis is limited to the first reactions of MAR; however, the significance of IC-MAR is strongly indicated.

© 2025 The Japan Society of Plasma Science and Nuclear Fusion Research

Keywords: molecular activated recombination, ion conversion, detached divertor, radio-frequency plasma, DT-ALPHA

DOI: 10.1585/pfr.20.1401015

## 1. Introduction

One of the most crucial problems in diverted tokamaks and stellarators is the safe handling of the power exhaust to the divertor plates. Fusion reactors will be operated in detached divertor mode, which is characterized by a reduction in plasma particle flux, to mitigate the heat load onto the divertor plates below an acceptable limit [1, 2]. Plasma volumetric recombination strongly contributes to detachment onset, and the recombination is classified into two types: electron-ion recombination (EIR) and molecular activated recombination (MAR). MAR was theoretically predicted and modeled [3, 4], and experimentally demonstrated [5] in the 1990s. Subsequently, studies on MAR have been enthusiastically conducted, particularly in linear divertor plasma simulators, *e.g.* NAGDIS-II [6, 7], MAP-II [8, 9], TPD-Sheet IV [10], ULS [11, 12], PISCES-A [13], GAMMA 10/PDX [14, 15], and Magnum-PSI [16].

As shown in Table 1, the main reaction chains of MAR in hydrogen plasma are DA-MAR and IC-MAR. DA and IC-MARs are attributed to the dissociative attachment and ion conversion, respectively. Both reactions are initiated by vibrationally excited hydrogen molecules, which are produced by electron impacts on ground electronic hydrogen molecules.

In tokamaks, energetic ions are periodically transported into the divertor region by edge-localized modes, causing

Table 1. Two main reaction chains of hydrogen molecular activated recombination.  $\nu$  and  $p$  represent the vibrational and principal quantum numbers, respectively.

Label	Reaction
DA-MAR	$\text{H}_2(\nu) + \text{e}^- \rightarrow \text{H}^- + \text{H}$ : Dissociative attachment $\text{H}^- + \text{H}^+ \rightarrow \text{H} + \text{H}^*$ ( $p = 2, 3$ ) : Mutual neutralization
IC-MAR	$\text{H}_2(\nu) + \text{H}^+ \rightarrow \text{H}_2^+(\nu) + \text{H}$ : Ion conversion $\text{H}_2^+(\nu) + \text{e}^- \rightarrow \text{H} + \text{H}^*$ ( $p > 2$ ) : Dissociative recombination

various collisions with hydrogen molecules and atoms. An experiment conducted with helium EIR plasma indicated that energetic ions decrease the reaction rate of EIR through the charge exchange reaction [17]. The influence of energetic ions on MAR is expected to be more complex. MAR can be facilitated by the production of  $\text{H}_2(\nu)$  via energetic ion collisions. In contrast, if energetic ions dissociate or ionize  $\text{H}_2(\nu)$ , the reaction rate of MAR decreases; thus, plasma detachment is impeded.

To investigate the complicated phenomena induced by energetic ions, we plan to conduct an ion beam injection experiment into hydrogen MAR plasma. Recently, we successfully produced hydrogen plasma with a rollover of the electron density and a monotonic decrease in the electron temperature [18]. This behavior occurs when volumetric recombination is strongly facilitated. However, the contributions of molecular reactions have not yet been analyzed in detail. In this study,

\*Corresponding author's e-mail: keigo.yoshimura.s5@dc.tohoku.ac.jp

we analyzed the first reactions of two MARs using Fulcher- $\alpha$  band spectroscopy to determine the significance of the MARs on the plasma particle loss observed in DT-ALPHA.

## 2. Experimental Setup

The steady-state radio-frequency (RF) plasma source DT-ALPHA [19] was used in the experiments. Figure 1(a) shows a schematic diagram of the DT-ALPHA device. The DT-ALPHA device consists of a quartz pipe and a stainless steel chamber. The total length of the device is approximately 2 m. The inner diameters of the quartz pipe and stainless steel chamber are 36 and 63 mm, respectively. The  $z$ -axis is defined as illustrated. An RF antenna is wound around the quartz pipe, and the antenna is connected to an RF power supply through a matching circuit. Plasma is produced with an RF discharge of 13.56 MHz. During the experiment, the RF power was maintained at approximately 620 W. A hydrogen working gas was supplied to the device near the upstream end. In addition, a hydrogen secondary gas was fed in the downstream region ( $z = 1.58$  m) to enhance the hydrogen MAR reactions. In this experiment, the hydrogen molecule pressure at  $z = 1.58$  m was increased up to 5 Pa by varying the amount of the secondary gas. Three orifice units are installed inside the device to suppress the diffusion of the secondary gas toward the plasma production region. The amounts of the working and secondary gases were controlled using mass-flow controllers. The hydrogen molecule pressures measured at  $z = 0.98$  and  $1.58$  m are denoted as  $p_{\text{up}}$  and

$p_{\text{down}}$ , respectively.

Measurements were performed near the plasma production region ( $z = 0.98$  m) and the secondary gas feeding position ( $z = 1.58$  m). At  $z = 0.98$  m, the electron temperature ( $T_e$ ) and electron density ( $n_e$ ) were measured using a Langmuir probe to confirm that these parameters were kept almost constant during the experiment. At the secondary gas feeding position, a Langmuir probe was also used to obtain  $T_e$  and  $n_e$ . In addition, the optical emissions of atomic hydrogen ( $H_\alpha$  and  $H_\beta$ ) and molecular hydrogen (Fulcher- $\alpha$  band) were collected using two spectroscopes. Figure 1(b) represents a cross-sectional view at  $z = 1.58$  m. The viewing chord can be moved vertically. In the following sections, the radial position of the plasma is denoted by  $r$ .

## 3. Results and Discussion

### 3.1 Electron density rollover at the secondary gas feeding position

The electron density and temperature were measured with various amounts of the hydrogen working and secondary gases. The Langmuir probes were radially movable but kept close to near  $r = 0$  mm during the measurements. Figure 2 summarizes the results as a function of  $p_{\text{down}}$ . Figures 2(a) and (b) show the flow rate of the working/secondary gases and  $p_{\text{up}}$ , respectively. Although there are two orifice units between  $z = 0.98$  and  $1.58$  m as shown in Fig. 1, it is difficult to completely control the diffusion of the secondary gas toward the upstream region. Therefore, the

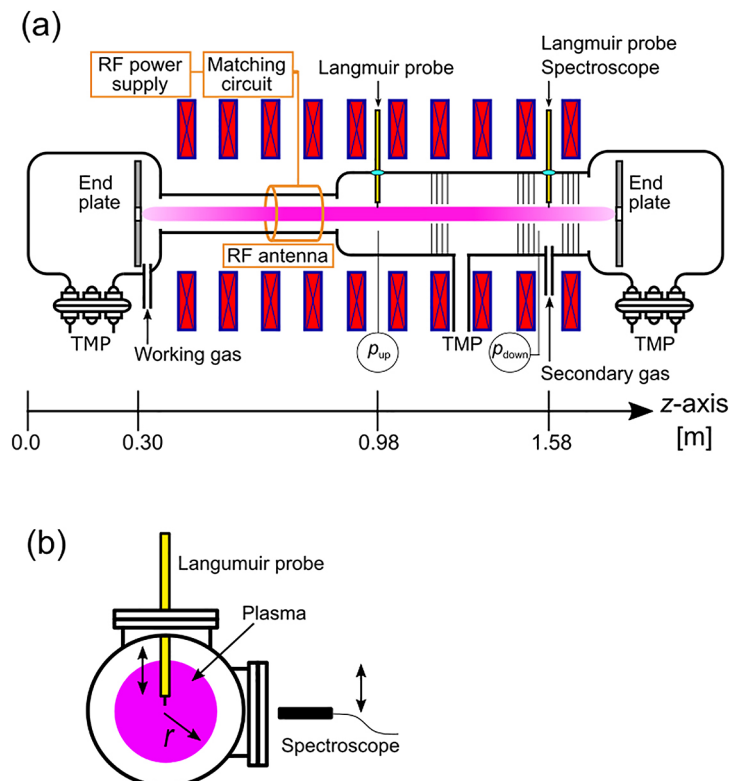


Fig. 1. Schematic of (a) DT-ALPHA device and (b) cross-sectional view at  $z = 1.58$  m.

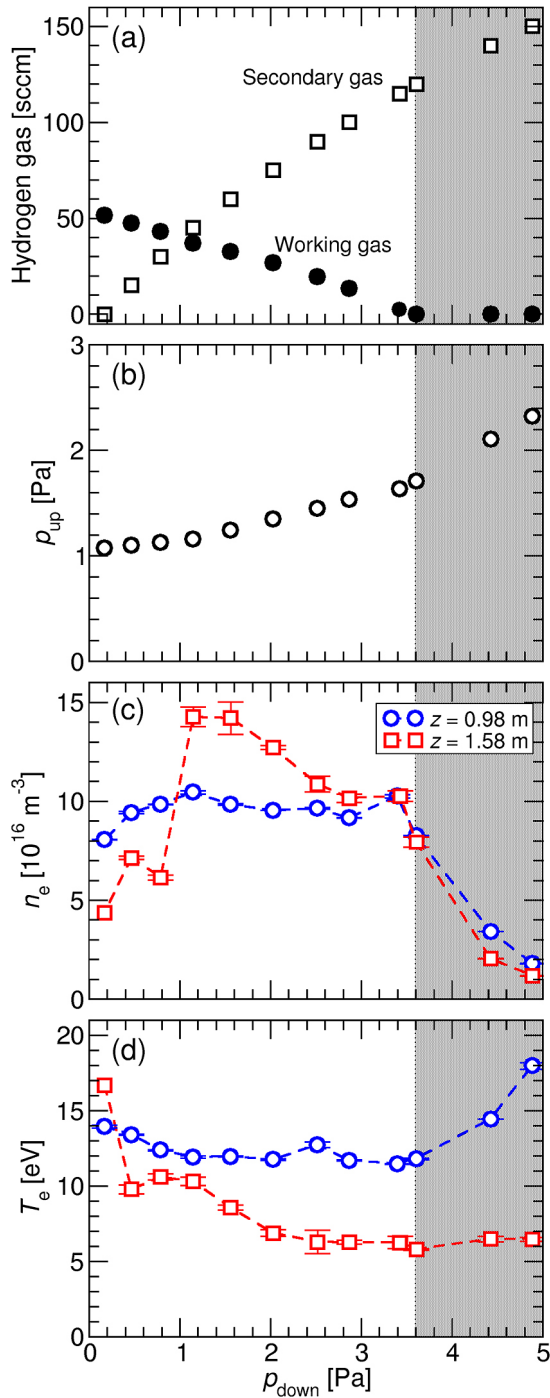


Fig. 2. (a) Amounts of working and secondary gases, (b) neutral pressure in upstream region, (c) electron density, and (d) electron temperature as functions of downstream pressure. Two Langmuir probes were kept close to  $r = 0$  mm. The results at  $p_{\text{down}} > 3.6$  Pa are ignored because the discharge mode was likely changed.

working gas flow rate was to be decreased as the secondary gas flow rate increased to maintain  $p_{\text{up}}$  approximately 1 Pa. The circles in Figs. 2(c) and (d) show  $n_e$  and  $T_e$  observed at  $z = 0.98$  m. Although  $p_{\text{up}}$  slightly increased with increasing  $p_{\text{down}}$ ,  $n_e$  and  $T_e$  were almost constant at  $1 \times 10^{17} \text{ m}^{-3}$  and 12 eV until  $p_{\text{down}} = 3.6$  Pa. For  $p_{\text{down}} > 3.6$  Pa, the flow rate of the working gas reached 0 sccm, leading to an undesirable increase in the upstream pressure. According to a previous

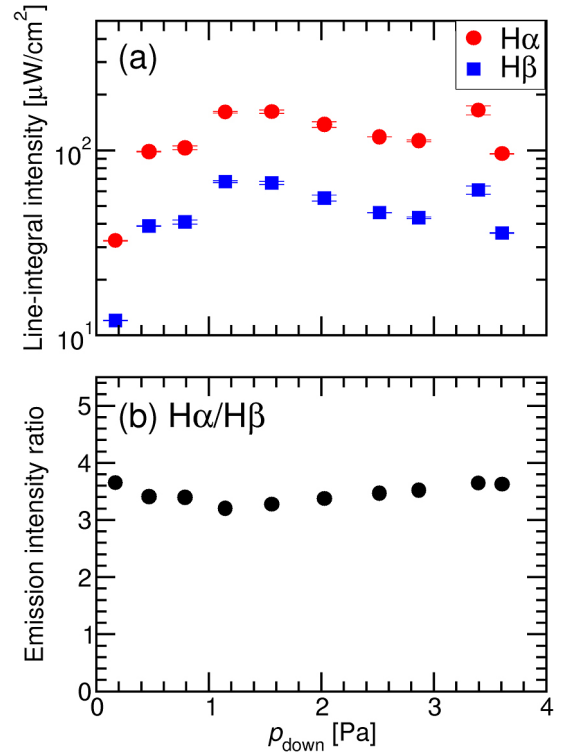


Fig. 3. (a) Emission intensities of  $H_{\alpha}$  and  $H_{\beta}$  and (b)  $H_{\alpha}/H_{\beta}$  ratio obtained at  $z = 1.58$  m as a function of downstream pressure.

study [20], when the neutral pressure increases excessively,  $n_e$  and  $T_e$  at  $z = 0.98$  m change dramatically, probably due to the change in the discharge modes. Therefore, the significant changes observed in  $n_e$  and  $T_e$  at  $p_{\text{down}} > 3.6$  Pa were likely associated with these changes. As shown in Fig. 2(c), ionization was facilitated at  $z = 1.58$  m by the increase in  $p_{\text{down}}$ , and  $n_e$  reached a maximum at 1.1 Pa. Subsequently, it decreased monotonically until 3.6 Pa.  $T_e$  decreased monotonically from approximately 17 to 6 eV. Because the electron temperature was too high for EIR, the rollover can be attributed to MAR.

### 3.2 Pressure dependence of emission intensity of Balmer series

The intensity ratio of  $H_{\alpha}$  and  $H_{\beta}$  is a good indicator of DA-MAR because it selectively produces hydrogen atoms excited into  $p = 2$  and 3 (Table 1).  $H_{\alpha}/H_{\beta}$  increases several-fold with the onset of the DA-MAR [14]. Therefore, the emission intensities of  $H_{\alpha}$  and  $H_{\beta}$  were collected at  $z = 1.58$  m. Figure 3(a) shows the results. Here,  $H_{\alpha}$  and  $H_{\beta}$  are line-integrated values along a viewing-chord crossing near the plasma axis. The intensities of  $H_{\alpha}$  and  $H_{\beta}$  increased similarly with increasing  $p_{\text{down}}$ . Figure 3(b) shows the  $H_{\alpha}/H_{\beta}$  ratio. No clear change was observed in the ratio even though  $p_{\text{down}}$  was increased up to 3.6 Pa, indicating that the contribution of DA-MAR to the density rollover was negligibly small.

However, the line-integration effect should be discussed because a cold recombining region occasionally surrounds a hot ionizing region, and the bright hot core dominates the

line-integrated emission. The radial profiles of the local line emission intensities for  $p_{\text{down}} = 0.8, 1.6, \text{ and } 3.4 \text{ Pa}$  were then evaluated by the Abel inversion. These pressures correspond to before the rollover, at the density peak, and after the rollover, respectively. Figures 4(a) and (b) show the radial profiles of the local emission intensities of the  $H_\alpha$  and  $H_\beta$  lines, respectively.  $H_\alpha$  and  $H_\beta$  exhibited similar radial profiles regardless of the neutral pressure. As shown in Fig. 4(c),  $H_\alpha/H_\beta$  ratio was spatially uniform and its shape was independent of the pressure even though the ratio was evaluated with local emissions. We conclude that the contribution of DA-MAR to plasma particle loss was negligible.

### 3.3 Reaction rates of ion conversion and dissociative attachment

To confirm the contribution of IC-MAR to the density rollover, the reaction rates of the ion conversion (IC) and dissociative attachment (DA) were evaluated. The cross-sections of IC and DA strongly depend on the vibrational excitation level of hydrogen molecules [21]. Therefore, the vibrational distribution was initially evaluated based on the Fulcher- $\alpha$  band spectroscopy, as described in Refs. [22] and [23].

Assuming coronal equilibrium for the excited hydrogen molecules, the emission intensity for the Fulcher- $\alpha$  band ( $d$ -state to  $a$ -state) is expressed as follows:

$$I_{av'J'}^{dv'J''} = \frac{hc}{\lambda} \frac{A_{av'J''}^{dv'J'}}{\sum_{v'',J''} A_{av'J''}^{dv'J'}} \sum_v \sum_J R_{XvJ}^{dv'J'} N_{XvJ}, \quad (1)$$

where  $(v', J')$  and  $(v'', J'')$  denote the vibrational and rotational quantum numbers at the upper and lower levels, respectively;  $A$  represents the spontaneous emission coefficient of the corresponding transition;  $R$  represents the electron impact excitation rate of hydrogen molecules from the ground electronic state  $(X, v, J)$  to the upper level of the Fulcher- $\alpha$  band  $(d, v', J')$ . The electron impact excitation rate was calculated based on the Gryzinski semi-classical theory [22]. Here,  $N_{XvJ}$  represents the ro-vibrational population of the ground electronic state. If  $N_{XvJ}$  follows the Boltzmann distribution, it can be expressed as follows:

$$N_{XvJ} = C_v(2J+1)g_{\text{as}} \exp \left[ -\frac{F_X(J, v)}{k_B T_{\text{rot}}} - \frac{\Delta G_X(v)}{k_B T_{\text{vib}}} \right], \quad (2)$$

where  $v$  and  $J$  represent the vibrational and rotational quantum numbers in the ground electronic state, respectively;  $C_v$ ,  $g_{\text{as}}$ ,  $T_{\text{rot}}$ , and  $T_{\text{vib}}$  denote the normalization constant, degeneracy for the considered nuclear spin, and rotational and vibrational temperatures, respectively;  $F_X(J, v)$  denotes the rotational energy, and  $\Delta G_X(v)$  denotes the energy difference between  $v = 0$  and the vibrational state of interest. Using  $N_{XvJ}$ , the vibrational distribution ( $N_{Xv}$ ) can be calculated as follows:

$$N_{Xv} = \sum_J N_{XvJ}. \quad (3)$$

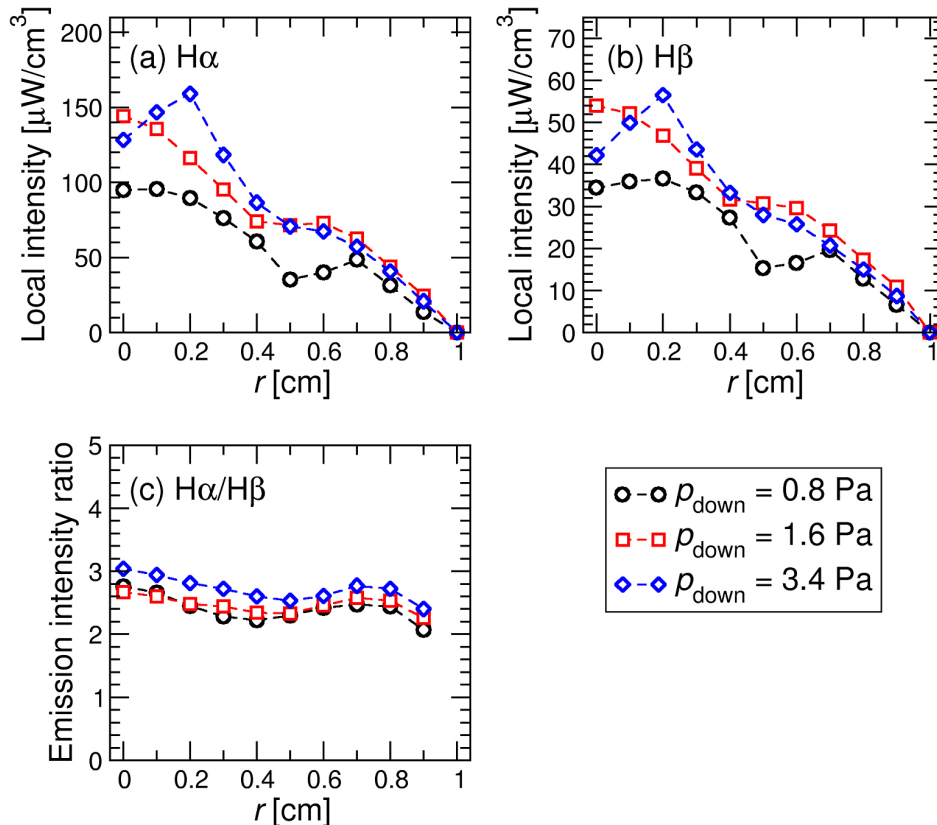


Fig. 4. Radial profile of (a) local emission intensity of  $H_\alpha$ , (b) local emission intensity of  $H_\beta$ , and (c) the  $H_\alpha/H_\beta$ .

Rotational and vibrational quantum numbers up to  $J = 10$  and  $v = 14$  were considered in the analysis.  $T_{\text{rot}}$  and  $T_{\text{vib}}$  were determined such that the relative intensity of the calculated Fulcher- $\alpha$  band emissions best reproduced the experimentally obtained intensity. Using  $T_{\text{rot}}$  and  $T_{\text{vib}}$ , the vibrational distribution of the excited hydrogen molecules was calculated using Eqs. (2) and (3). Finally, the reaction rates of IC ( $R_{\text{IC}}$ ) and DA ( $R_{\text{DA}}$ ) can be obtained as follows:

$$R_{\text{IC}} = \sum_v N_{Xv} n_{\text{H}^+} \langle \sigma_{\text{IC}} V \rangle, \quad (4)$$

$$R_{\text{DA}} = \sum_v N_{Xv} n_e \langle \sigma_{\text{DA}} V \rangle, \quad (5)$$

where  $n_{\text{H}^+}$  denotes the proton density, and we assumed that  $n_{\text{H}^+}$  is equal to the electron density. Since molecular ions also exist in hydrogen plasma, the assumption likely overestimated  $n_{\text{H}^+}$  by several times. However, this has no significant influence on the analysis because, as shown later,  $R_{\text{IC}}$  is significantly greater than  $R_{\text{DA}}$ .  $\sigma_{\text{IC}}$  and  $\sigma_{\text{DA}}$  represent cross-sections of IC and DA, respectively [21]. Vibrational levels up to 14 were considered for the cross-sections. Here,  $V$  represents the relative velocities of protons/electrons to the excited molecules. The thermal velocity was denoted as  $V$  in this analysis. The electron thermal velocity was calculated using  $T_e$ ; however,  $T_i$  was assumed because it was not measured. Since DT-ALPHA has no active ion heating and ions rapidly lose their energy through the charge exchange reaction, we assumed  $T_e/10 \leq T_i \leq T_e/2$ . The ionization reaction rate ( $R_{\text{ion}}$ ) was also analyzed because the density rollover can be explained if  $R_{\text{ion}}$  decreases as  $p_{\text{down}}$  increases. Using the collisional-radiative model for atomic hydrogen [24],  $R_{\text{ion}}$  was evaluated as  $R_{\text{ion}} = S_{\text{CR}} n_e n_{\text{H}}$ . Here,  $S_{\text{CR}}$  and  $n_{\text{H}}$  denote the CR ionization rate coefficient and the ground state atomic hydrogen density, respectively. The diagnostic of  $n_{\text{H}}$  was not available; thus, we evaluated  $n_{\text{H}}$  through the density ratio of atomic and molecular hydrogen, as reported in Ref. [8]. Although the experiment in Ref. [8] was conducted with a helium-hydrogen mixture plasma, we referred to this report because the neutral pressure,  $n_e$ , and  $T_e$  were similar to those

in the present experiment.  $n_{\text{H}}/n_{\text{H}_2}$  was approximately  $10^{-2}$  when  $n_e$ ,  $T_e$ , and the total neutral pressure were  $0.7 \times 10^{17} \text{ m}^{-3}$ , 3 eV, and 1.2 Pa, respectively [8].  $n_{\text{H}}/n_{\text{H}_2}$  changes only 50 % even though  $n_e$  changed by one order of magnitude. Therefore, we assumed that  $n_{\text{H}}/n_{\text{H}_2}$  was constant at  $10^{-2}$  in the present analysis.

Figure 5 shows a typical Fulcher- $\alpha$  band spectrum collected at  $z = 1.58 \text{ m}$ . Twelve line spectra corresponding to (0-0)Q1 to (3-3)Q3 were clearly observed. The numbers in parentheses are the vibrational quantum numbers of the upper and lower states. Q indicates that the rotational quantum number ( $J$ ) does not change before and after the transition:  $\Delta J = 0$ . The number next to Q represents the rotational quantum number of the upper and lower states. In Fig. 6, the vibrational temperature and distribution are plotted.  $T_{\text{vib}}$  slightly increased as  $p_{\text{down}}$  increased and reached its maximum at approximately  $p_{\text{down}} = 0.5 \text{ Pa}$ . As shown in Fig. 2(d), the electron temperature in the downstream region decreased at approximately this pressure. Therefore, the slight increase in  $T_{\text{vib}}$  can be attributed to energy transfer from the bulk electrons to the hydrogen molecules. Subsequently,  $T_{\text{vib}}$  exhibited a monotonic decrease from approximately 3500 K to 2400 K with increasing  $p_{\text{down}}$ . The vibrational distributions for  $p_{\text{down}} = 0.5, 1.1, \text{ and } 3.4 \text{ Pa}$  are shown in Fig. 6(b).  $T_{\text{vib}}$  at 0.5 and 1.1 Pa are almost the same; thus, the vibrational distributions corresponding to these pressures are also almost the same. In contrast,  $T_{\text{vib}}$  at 3.4 Pa is approximately 700 K lower than that at the other two pressures; thus, the distribution is significantly different, particularly at high vibrational levels. Figure 7 shows the reaction rates of IC, DA, and ionization as functions of  $p_{\text{down}}$ . To discuss the contributions of the two MAR reactions and ionization to the density rollover, the electron density obtained at  $z = 1.58 \text{ m}$  is also plotted in Fig. 7 with open squares. Initially, the ionization reaction rate increased with  $p_{\text{down}}$  and reached a maximum at 1.1 Pa. The increase in  $n_e$  at approximately 1 Pa can be explained by the enhanced ionization. The reaction rate of IC was two orders of magnitude greater than that of DA. Furthermore, although it was within the error bar range, the reaction rate of IC was several times larger than that of ionization and

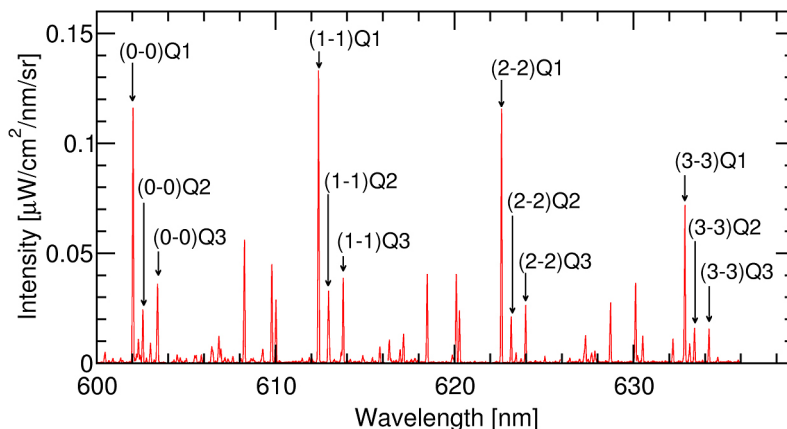


Fig. 5. Typical Fulcher- $\alpha$  band spectrum observed at  $z = 1.58 \text{ m}$ .

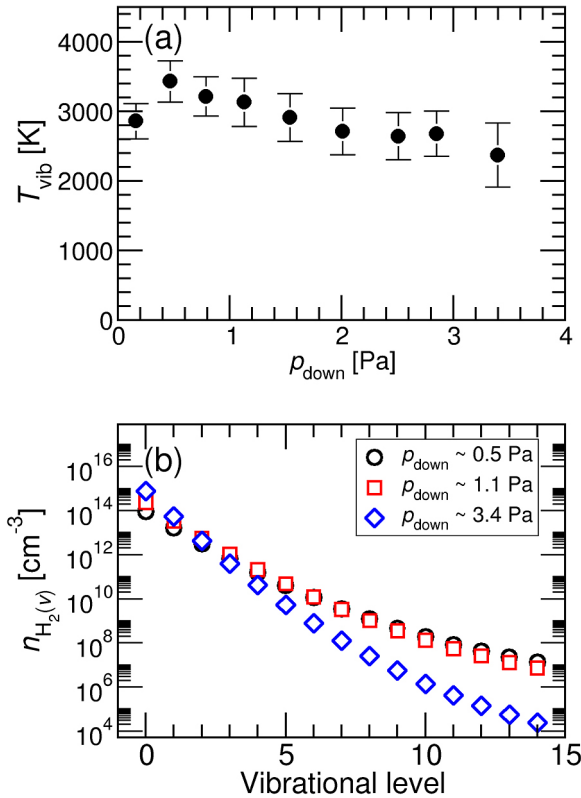


Fig. 6. (a) Vibrational temperature and (b) vibrational distribution of hydrogen molecules in ground electronic state.

remained high even when the electron density decreased. In particular, at  $2.0 \text{ Pa} < \rho_{\text{down}} < 3.4 \text{ Pa}$ , the reaction rate of ionization was almost constant. Therefore, a decrease in the ionization rate is unlikely to explain the rollover. These results indicate that IC-MAR strongly contributes to volumetric plasma particle loss rather than DA-MAR and decrease in the ionization rate, which is consistent with other reports [16, 25].

Plasma particle loss could have occurred not only by volumetric recombination but also by radial transport [26]. However, the particle flux due to radial transport evaluated with the same manner described in Ref. [25] decreased at  $\rho_{\text{down}} > 1.6 \text{ Pa}$ , indicating that it was less important than the MAR in the present study. But this calculation is a simplified one; thus, we plan to measure the radial particle flux for further understanding.

## 4. Conclusions

The contributions of MAR to the plasma particle loss in the hydrogen plasma produced in the DT-ALPHA device were analyzed in terms of the dissociative detachment (DA) and the ion conversion (IC) reaction rates. The rollover of the electron density and the monotonic decrease in the electron temperature were observed as the amount of the secondary gas increased. Regardless of the line-integration effect,  $H_{\alpha}/H_{\beta}$  ratio exhibited no pressure dependence and was distributed uniformly, indicating that the contribution of DA-MAR to the density rollover was negligible. Next, the reaction rates

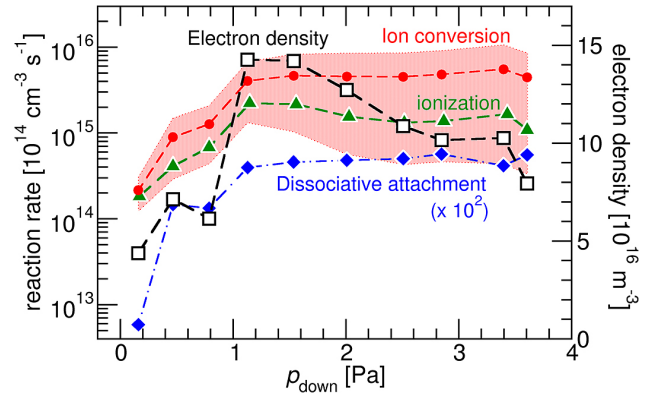


Fig. 7. The reaction rates of the ion conversion, the dissociative attachment, and ionization as functions of downstream pressure. The electron density at the same axial position is also plotted. The error bars of the reaction rate of the ion conversion are due to the ion temperature ( $T_i$ ), which was assumed to be in the range  $T_e/10 \leq T_i \leq T_e/2$ . The circles of ion conversion represent average values.

of IC and DA were evaluated based on the Fulcher- $\alpha$  band spectroscopy. The IC reaction rate was two orders of magnitude greater than the DA reaction rate. Although it was within the error bar range, the IC reaction rate was larger than the ionization reaction rate and remained high even when the electron density decreased. A decrease in the ionization rate is unlikely to explain the rollover because the reaction rate of ionization was almost constant. This analysis was limited to the first reactions of MARs. Further analysis of the second reactions is required to understand the contributions to the observed rollover. However, the significance of IC-MAR is strongly indicated.

To evaluate the reaction rates of the entire MAR process, analysis of a collisional radiative code for hydrogen molecules [27] is required. In addition, to investigate the contribution of radial transport, we plan to measure the radial particle flux. These analyses are currently ongoing, and the results will be reported elsewhere.

## Acknowledgments

I would like to thank Tomohiro Seino, Akihiro Kanno, and Yusaku Takahashi for their useful discussions. This work was supported by JSPS KAKENHI Grant Numbers JP24K00607 and JST Grant Number JPMJFS2102.

- [1] A. Loarte *et al.*, Nucl. Fusion **47**, S203 (2007).
- [2] N. Asakura *et al.*, Nucl. Fusion **57**, 126050 (2017).
- [3] S.I. Krasheninnikov *et al.*, Phys. Lett. A **214**, 285 (1996).
- [4] A. Yu. Pigarov *et al.*, Phys. Lett. A **222**, 251 (1996).
- [5] N. Ohno *et al.*, Phys. Rev. Lett. **81**, 818 (1998).
- [6] N. Ezumi *et al.*, J. Nucl. Mater. **266**, 337 (1999).
- [7] D. Nishijima *et al.*, Plasma Phys. Control. Fusion **44**, 597 (2002).
- [8] S. Kado *et al.*, J. Nucl. Mater. **337**, 166 (2005).
- [9] A. Okamoto *et al.*, J. Nucl. Mater. **363**, 395 (2007).
- [10] A. Tonegawa *et al.*, J. Nucl. Mater. **313**, 1046 (2003).

- [11] P.K. Browning *et al.*, *J. Nucl. Mater.* **337**, 232 (2005).  
[12] B. Mihaljčić *et al.*, *Phys. Plasmas* **14**, 013501 (2007).  
[13] L. Cai *et al.*, *Phys. Plasmas* **15**, 102505 (2008).  
[14] M. Sakamoto *et al.*, *Nucl. Mater. Energy* **12**, 1004 (2017).  
[15] N. Ezumi *et al.*, *Nucl. Fusion* **59**, 066030 (2019).  
[16] G.R.A. Akkermans *et al.*, *Phys. Plasmas* **27**, 102509 (2020).  
[17] H. Takahashi *et al.*, *Phys. Plasmas* **23**, 112510 (2016).  
[18] K. Yoshimura *et al.*, *Plasma Fusion Res.* **17**, 1201082 (2022).  
[19] A. Okamoto *et al.*, *Plasma Fusion Res.* **3**, 059 (2008).  
[20] T. Seino *et al.*, *Plasma Fusion Res.* **15**, 1201056 (2020).  
[21] R.K. Janev *et al.*, *Julich JUEL-4105* (2003).  
[22] B. Xiao *et al.*, *Plasma Phys. Control. Fusion* **46**, 653 (2004).  
[23] Y. Kuwahara *et al.*, *Plasma Fusion Res.* **2**, S1081 (2007).  
[24] A. Okamoto *et al.*, *AIP Conf. Proc.* **2319**, 030007 (2021).  
[25] R. Chandra *et al.*, *Nucl. Mater. Energy* **34**, 101360 (2023).  
[26] E.M. Hollmann *et al.*, *Phys. Plasmas* **8**, 3314 (2001).  
[27] K. Sawada and M. Goto, *Atoms* **4**, 29 (2016).